Cyclic loading of an idealized clay-filled fault; comparing hydraulic flow in two clay gouges.

Robert Cuss, Caroline Graham, Andrew Wiseall, Jon F. Harrington, British Geological Survey, Keyworth, Nottingham, NG12 5GG, UK

Corresponding author: R.J. Cuss, British Geological Survey, Keyworth, Nottingham, NG12 5GG, UK. (rjcu@bgs.ac.uk)

Abstract: *The flow of water along discontinuities, such as fractures or faults, is of paramount importance in understanding the hydrogeology of many geological settings. An experimental study was undertaken comprising two experiments on a 30° slip-plane filled with kaolinite or Ball Clay gouge using a bespoke Angled Shear Rig (ASR). The gouge was initially loaded in equal step changes in vertical stress, followed by unloading of the sample in similar equal steps. This was followed by reloading to a new maximum stress, followed by unloading; the test history was therefore load-unload-reload-unload (LURU). The transmissivity of the kaolinite and Ball Clay gouge showed a power-law relationship with vertical stress. The LURU history showed considerable hysteresis, with flow effectively unchanged during unloading, even when vertical stress was close to zero. Reloading resulted in flow similar to that seen during unloading suggesting that the unloading-reloading path is similar to the rebound-reconsolidation line in classic soil mechanics. These observations show the importance of stress history on fracture flow; consideration of just the current stress acting upon a fracture may result in inaccuracies of predicted hydraulic flow. Once a new stress maximum was achieved the transmissivity of the fracture continued to reduce. No significant variation was seen in the flow response of kaolinite and Ball Clay gouge suggesting that the*

inclusion of illite and quartz did not have a significant influence on the form of the relationship between stress and flow, i.e. both described by a power-law.

Keywords

Fracture flow; hydraulic flow; kaolinite; Ball Clay; shear testing; stress history; carbon capture and storage.

1.0 Introduction

Discontinuities (fracture, faults, joints, interfaces, etc.) play a pivotal role in controlling the movement of water and gas in many geological settings. Depending on their orientation, displacement, mineral composition and stress regime discontinuities can be the controlling structural feature retarding the flow of hydrocarbons in conventional environments, containing super-critical CO_2 in sequestration projects, and movement of gas and/or water in radioactive waste disposal. Discontinuities can vary significantly in age. Normal faults acting as hydrocarbon traps may have formed millions of years ago, whereas subsidence induced faulting/fracturing in the same basin will have formed during the depletion of the reservoir. Therefore in many geological settings both natural and induced discontinuities will have formed.

Fluid flow in argillaceous materials, whether through the bulk rock or along discontinuities, is closely related to the mechanical state of the caprock. In particular, the role of faults and fractures as potential conduits or barriers to fluid flow is likely to be of critical importance to seal integrity in Carbon Capture and Storage (CCS) sites. In addition, recent studies [Zoback & Gorelick, 2012] and on-going developments relating to induced seismicity [Green, *et al.* 2011] in other industries have also highlighted the importance of a thorough understanding of the potential for, and controls on, fault reactivation behavior.

In particular, fault-sealing of caprocks is likely to be heavily influenced by the presence of clays along the slip surface. The sealing properties of inactive faults are well known in the hydrocarbons industry and may arise through the presence of clay-rich gouge or through hydrothermal cementation. For fault-valve behavior to take place, a fault must cut across a vertical fluid pressure gradient which exceeds the hydrostatic gradient. The fault becomes conductive when shear stress and/or pore pressure is sufficient. The consequent upward discharge of fluids along the fault from the overpressured zone continues until the entire hydraulic gradient reverts to hydrostatic conditions, or until the fault reseals. This also alters the frictional shear resistance across the impermeable barrier.

Faulted geological settings are complex systems that are borne out of multiple episodes of deformation, in the form of faulting, subsidence and exhumation, and altered stress regimes. This means that faults cannot be viewed as static features over geological time. Nor can they be considered static on CO_2 injection time scales, as complex pore-pressure histories and chemical alteration-driven deformation may also have an impact on caprock systems. As such, time is a significant factor in fault sealing.

On the long time-scales of interest in CCS, cross-reservoir fluid migration may lead to changes in stress-state long after injection ceases. The response of new or previously-sealed discontinuities exposed to these dynamic conditions, may be significant. Noy *et al.* [2012] demonstrated that pore-pressure perturbations, resulting from the injection of CO_2, may persist for significant periods (~300 years) after the injection phase. These perturbations are likely to be particularly large in magnitude within the immediate vicinity of injection, but are also demonstrably of concern 'a considerable distance outside the CO_2 footprint at the end of the injection period'. This raises a number of uncertainties in relation to the interaction of fluids with caprock faulting, including the role of: (i) pre-existing discontinuities in the caprock (either natural or reservoir-depletion-induced) with the potential to transmit fluids

under an elevated pore-pressure condition, (ii) critically oriented faults with the potential for reactivation (as compared to those far from critically stressed), or faulting with the potential for infrequent but significant seismicity.

Additionally, both near- and far-field discontinuities may be exposed to a range of changing fluid chemistries during the evolution of a storage site, from CO_2-rich fluids to the migration of brines at the periphery of the pressure pulse. In contrast to reservoir rocks, the phenomenon of clay swelling is of major importance to the sealing behavior of argillaceous cap-rocks [Horseman *et al.*, 2005; Tsang *et al.*, 2005], with the potential to notably affect transmissivity of discontinuities. CO_2 has been shown to markedly impact on the swelling properties of clays [Espinoza & Santamaria, 2012], but there is a paucity of data relating to the impact on shale swelling properties and, in particular, the potential effects for fault sealing behavior.

The permeability of rocks has been widely reported under hydrostatic stress conditions [e.g. Zoback and Byerlee 1975; Walsh and Brace 1984; Morrow *et al*., 1984; David *et al*., 1994; Dewhurst *et al*., 1999[a,b]; Katsube, 2000; Katsube *et al*., 1996 [a,b]; Kwon *et al*., 2001; Neuzil *et al*., 1984 etc] in order to establish the relationship between effective stress and permeability for different rock types. However, in the field, rocks are normally subjected to an anisotropic stress-field, where the vertical stress (determined by the weight of the overburden) exceeds the two horizontal stresses [Holt, 1990]. This has led to investigations of the sensitivity of matrix permeability to non-hydrostatic stress conditions, especially in sandstones [e.g. Keaney *et al*., 1998; Zhu and Wong, 1994; Zhu and Wong, 1997]. The reported permeability for intact shale, mudstones, and clay aggregates subjected to hydrostatic pressures varies from 10^{-16} m^2 to 10^{-23} m^2 [Kwon *et al*., 2001]. Many researchers have shown that the permeability of shale decreases with externally applied stress [Dewhurst *et al*., 1999[a,b]; Katsube, 2000; Katsube *et al*., 1996[a,b]; Kwon *et al*., 2001; Neuzil *et al*., 1984] and decreased

99 porosity [Dewhurst *et al*., 1998; Schloemer and Kloss, 1997]. A number of non-linear
100 relationships have been proposed between permeability, porosity, and pressure in shale and
101 mudstones, including exponential and power laws between permeability and pressure
102 [Dewhurst *et al*., 1999a; Katsube *et al*., 1991].

103 Gutierrez *et al*. [2000] investigated experimentally the hydromechanical behavior of an
104 extensional fracture in Kimmeridge Shale under normal and shear loading. It was shown that,
105 at the time it was created, the fracture probably had about nine orders of magnitude higher
106 permeability than the permeability of the intact shale. Increasing the normal stress across the
107 fracture reduced the fracture permeability following an empirical exponential law. However,
108 loading the sample to an effective normal stress twice as much as the intact rock unconfined
109 compressive strength did not completely close the fracture, although it did reduce the
110 permeability by an order of magnitude. Cuss *et al.* [2011] showed that fracture transmissivity
111 in Opalinus Clay (OPA) decreased linearly with an increase in normal load over a limited
112 stress range. This study also showed that shearing was an effective self-sealing mechanism in
113 OPA and reduced hydraulic fracture transmissivity to similar levels to that of the intact
114 material. Cuss *et al.* [2014[a,b]] reported a one order of magnitude reduction in fracture
115 transmissivity of OPA just in response to re-hydration of the fracture. A further order of
116 magnitude reduction was observed in response to shearing along the fracture.

117 The current study represents the first stage of a three-part investigation of the potential for
118 fault reactivation during the sequestration of carbon dioxide. The three parts of the study
119 were; 1) the role of stress history on fault flow properties; 2) quantification of fault
120 reactivation potential as a result of elevated pore pressure; and 3) the role of stress history on
121 fault reactivation. As a consequence of part (2) of the experimental program, the current
122 reported study investigated the hydraulic flow properties of a clay-filled discontinuity at 30°
123 to horizontal to cyclic changes in vertical load. Two clay gouges were selected so as to

investigate any potential changes in fault reactivation potential in part (2) of the study. The objectives of the current study were:

- Investigate the relationship between stress and fault transmissivity;
- Investigate the role of stress history on fault transmissivity;
- Compare results from two clay gouges (kaolinite and Ball Clay).

This would simulate effective stress changes, such as pore-pressure variations on faults during CO_2 sequestration or stress relaxation through exhumation. Previous experimental work at the British Geological Survey (BGS) on fracture transmissivity in Opalinus clay [Cuss *et al.*, 2009; 2011; 2014[a,b]] and kaolinite gouge [Sathar *et al.*, 2012] showed that hydraulic flow is a complex, focused, transient property that is dependent upon normal stress, shear displacement, fracture topology, fluid composition, and clay swelling characteristics. The current experimental program aimed to extend this knowledge by investigating the influence of vertical stress cycling on hydraulic flow through gouge filled discontinuities.

Perturbations of the stress field are likely in many geological scenarios and the influence this has on the flow properties of faults is important in determining the hydrogeological response of the subsurface. This study was aimed to answer the question of whether stress history is of importance in fault flow and whether the current stress state will dictate the flow properties of faults. The study also aimed to answer whether variations in pore pressure as a result of CO_2 sequestration would alter the transport properties of existing faults within reservoirs. Should stress history be observed, the flow properties of the faults would be dictated by the stress state at which they were formed, not necessarily the current stress state and this adds confidence that pore pressure variations during sequestration would not result in leakage.

2.0 Experimental setup

147 All experiments were performed using the bespoke Angled Shear Rig (ASR, Figure 1)
148 designed and built at the BGS. Previous experiments conducted on Opalinus Clay [Cuss *et*
149 *al.*, 2009; 2011; 2014] showed that fracture topology is a key parameter in controlling fluid
150 flow along fractures. In order to reduce the number of variables required to fully understand
151 flow, a "generic" discontinuity with smooth fracture surfaces was investigated.

152 The ASR (Figure 1) comprised of 5 key components:

153 1. Rigid body that had been designed to deform as little as possible during the experiment;

154 2. Vertical load system comprising an Enerpac hydraulic ram that was controlled using a
155 Teledyne/ISCO 260D syringe pump, a rigid loading frame and an upper thrust block
156 (with capacity of up to 20 MPa vertical stress, 72 kN force). The Enerpac ram had a
157 stroke of 105 mm, which meant that it could easily accommodate the vertical
158 displacement of the top block as it rode up the fault surface at constant vertical load.
159 Note: The vertical stress created by the ram is not equal to the normal stress perpendicular
160 to the fault plane and represents the maximum principal stress within the reservoir;

161 3. Shear force actuator comprised of a modified and horizontally mounted Teledyne/ISCO
162 500D syringe pump designed to drive shear as slow as 14 microns a day at a constant rate
163 (equivalent to 1 mm in 69 days) along a low friction bearing. Note that no shearing was
164 conducted in the current study;

165 4. Pore pressure system comprising a Teledyne/ISCO 500D syringe pump that could deliver
166 either water up to a pressure of 25.8 MPa. The syringe pump delivered water through the
167 center of the top block directly to the fault surface.

168 5. A state-of-the-art custom designed data acquisition system using National Instruments
169 LabVIEW™ software facilitating the remote monitoring and control of all experimental
170 parameters.

The experimental fault assembly consisted of precision machined 316 stainless steel top and bottom blocks (thrust blocks) with a dip of 30 degrees with respect to horizontal. The thrust blocks were polished so as not to introduce preferential pathways for flow. The top block was connected to the vertical loading arrangement by means of a swivel mechanism which was engaged to the shoulders on either side of the top block. Care was taken in the design of the swivel mechanism so as to negate rotation and tilting of the top blocks and shear mechanism. Two pore pressure transducers, attached to ports which were positioned orthogonally to each other at 15 mm from the central pore fluid inlet, allowed measurement of pore pressures within the fault gouge (see Figure 1). The thrust blocks of the apparatus were made with a contact area of 60 mm × 60 mm. The lower thrust block was longer than the top one so that the contact area of the experimental discontinuity could be maintained constant during a shear test.

Vertical movement of the upper thrust block was measured by a high precision non-contact capacitance displacement transducer, which had a full range of ± 0.5 mm and an accuracy of 0.06 µm. Horizontal load was measured using a load cell fitted laterally to the top-block. This measured the force resultant from lateral movement of the bottom block transmitted through the clay gouge.

Gouge material for the experiments was prepared from either powdered kaolinite or Ball Clay (as described in Table 1); 16 ± 0.1 g of de-ionized water was added to 20 ± 0.1 g of oven dried clay powder. The water and clay were then stirred for five minutes giving a fully saturated paste. The mixed paste was smeared uniformly onto the surface of the top block, which was then carefully lowered onto the bottom block thus forming a paste gouge. The initial thickness of the gouge is usually of the order of 1 mm. However, as no lateral confinement was made of the clay gouge, thickness decreased to approximately 70 ± 10 µm with loading up to 10 MPa and clay was squeezed from between the thrust blocks; this excess

material stopped water from the shear bath entering the fault gouge or causing. The apparatus was designed without lateral gouge confinement as this would require sealing elements that would have a high frictional component along the fault surface compared with the low frictional properties of the clay.

Two experiments are described in this paper (Table 2). Both were conducted from a low vertical stress of approximately 0.4 MPa up to a maximum of 10 MPa. Each step was approximately 1 day in length, with vertical stress increased instantaneously. Steady-state flow had been achieved during this time, as seen by a constant transmissivity. Experience from previous studies [Sathar *et al.*, 2012] showed that this length was sufficient and is an appropriate compromise between overall test duration and attainment of stead-state flow. Throughout the experiment deionized water was injected at a pore pressure of 1 MPa by means of an ISCO/Teledyne syringe pump. The volume of the pump was monitored, giving information on the flow rate of the injection system. Flow rate could then be converted to transmissivity for the clay gouge. Fracture transmissivity is calculated assuming radial flow from the injection hole given the steady state fluid flow rate Q and the pressure head H at the injection point. Steady flow in a cylindrical geometry is given by:

$$Q = \frac{2\pi T\left(h_i - h_0\right)}{\ln\left(r_o\right) - \ln\left(r_i\right)} \qquad \text{Equation 1}$$

where T is the transmissivity, h_i is the head on the inner surface with radius r_i, and h_o is the head on the outer surface at radius r_o (Gutierrez *et al.*, 2000). For the current experimental setup r_0 = 30 mm, r_i = 1.96 mm, h_0 = 0.05 m (5 cm depth of water in the ASR bath) and h_i ~ 100 m (1 MPa injection pore pressure). Substituting these values into equation 1 and rearranging allows transmissivity ($m^2 s^{-1}$) to be simply calculated from:

$$T = 1.183 \times 10^{-12} \frac{Q}{P_p} \qquad \text{Equation 2}$$

if the fluid flux (Q in µl h^{-1}) and pore pressure (P_p in kPa) are known. This relationship was used to calculate the transmissivity of the fracture throughout the experiment. Average flowrate and standard deviation for each step was calculated from six hours of flow data prior to the final hour of each step.

3.0 Experimental results

Two tests with a test history of load-unload-reload-unload (LURU) are reported here, both conducted on a 30° slip-plane (Table 2).

Figure 2 shows the data recorded during the LURU experiment for test ASR_BigCCS_01 conducted on kaolinite clay gouge. The test consisted of 44 stages. Vertical stress was sequentially increased in stages of approximately 0.4 or 0.8 MPa per day to a maximum vertical stress of 6.5 MPa (Figure 2a). During the unloading stage the vertical stress was reduced in 0.2, 0.4 or 0.8 MPa steps per day to 0.1 MPa. This was followed by reloading in 0.4, 0.8 or 2 MPa steps to a vertical stress of 10 MPa, followed by unloading in 0.1, 0.4, 0.8 or 1.3 MPa steps to 0.1 MPa. The pore fluid injection pressure was maintained at a constant value of 1 MPa. Temperature varied between at 20.4 and 21.1 °C throughout the duration of the experiment, although this did not affect the experimental results (Figure 2b). The flow rate decreased by a factor of 6 from 87 µl h^{-1} to 15 µl h^{-1} during loading from 0 to 6.5 MPa (Figure 2c,d). Each test stage was approximately 1 day in duration. Previous studies [e.g. Sathar *et al.*, 2012] had shown that this was sufficient to achieve steady-state conditions. Ideally test stages should have been longer given the sensitivity of the Teledyne/ISCO pumps to resolve such low flows. However, a compromise had to be taken to obtain data within a realistic timeframe. During unloading from 6.5 to 0.1 MPa, flow rate remained essentially

241 unchanged at 14.8 µl h^{-1}. During the first stage of reloading from 0.1 to 2 MPa, flow reduced
242 from 14.8 µl h^{-1} to 9.4 µl h^{-1}, however, during reloading to the previous maximum stress of
243 6.4 MPa flow only marginally reduced from 9.4 µl h^{-1} to 9 µl h^{-1}. Continued loading
244 following attainment of a stress condition greater than previously experienced resulted in
245 flow reducing to approximately 6.5 µl h^{-1}. During the second unloading cycle to 0.1 MPa
246 flow did not recover until vertical stress was lower than 0.4 MPa, with flow increasing to
247 only 8.7 µl h^{-1} at a low vertical stress of 0.1 MPa. Pore pressure within the slip plane recorded
248 much lower pressures (6 – 26 kPa and 0 – 8 kPa) than the injection pressure (1 MPa) (Figure
249 2e), with P_1 initially decreasing during the first ten days of the experiment. Fracture width
250 reduced from an initial 160 µm to approximately 80 µm during the initial loading history
251 (Figure 2f). As seen, this reduction in fracture thickness is fully recovered during unloading.
252 The second loading stage reduced the fracture thickness to 60 µm, with full recovery
253 observed again. This suggests that no loss of gouge occurred following the initial loading
254 step.

255 Figure 3 shows the data recorded during the LURU experiment for test ASR_BigCCS_02
256 conducted on Ball Clay gouge. The test consisted of 34 stages. Vertical stress was
257 sequentially increased in stages of approximately 0.4 or 0.8 MPa per day to a maximum
258 vertical stress of 6.4 MPa (Figure 3a). During the unloading stage the vertical stress was
259 reduced in 0.4 or 0.8 MPa steps per day to 0.4 MPa. This was followed by reloading in 0.4 or
260 0.8 MPa steps to a vertical stress of 8.5 MPa, followed by unloading in 1 or 2 MPa steps to
261 0.4 MPa. The pore fluid injection pressure was maintained at a constant value of 1 MPa.
262 Temperature remained relatively uniform at 19.5 ± 0.1 °C throughout the duration of the
263 experiment, although a step in temperature was seen around Day 20 that did not affect the
264 experimental results (Figure 3b). The flow rate decreased by a factor of 4 from 40 µl h^{-1} to 9
265 µl h^{-1} during loading from 0 to 6.5 MPa (Figure 3c,d). During unloading from 6.5 to 0.4 MPa,

flow rate remained essentially unchanged from 9 µl h^{-1} to 8.6 µl h^{-1}. During reloading from 0.4 MPa to the previous maximum stress of 4.6 MPa, flow remained approximately constant, until a stress condition greater than previously experienced, with flow decreasing to 6.7 µl h^{-1}. During the second unloading cycle to 0.4 MPa flow did not recover, even at low vertical stresses. Pore pressure within the slip plane recorded much lower pressures (32 – 38 kPa) than the injection pressure (1 MPa) and were generally stable throughout the experiment (Figure 3e). Figure 3f shows that fracture thickness was initially 210 µm in thickness, with initial loading reducing this to approximately 60 µm. Unloading of the fault only recovered thickness to 75 µm. Reloading resulted in fracture thickness reducing to 35 µm, with a recovery to 53 µm. Both unloading stages did not fully recover fracture thickness, suggesting that gouge and/or water was expelled during the test history.

Figure 4 shows the results of flow achieved for two tests conducted injecting water into a 30° discontinuity during initial loading and unloading stages. As can be seen, the reduction in transmissivity (T) during increasing vertical stress (σ_v) can be described by the following power-law relationships:

Kaolinite: $T = 3.809\ \sigma_v^{-0.415}$ $R^2 = 0.979$

Ball Clay: $T = 2.659\ \sigma_v^{-0.514}$ $R^2 = 0.985$

Table 3 shows R^2 values for the fit of data for both tests using cubic, exponential, linear, logarithmic, and power-law relationships; all of which have previously been proposed to describe the relationship between stress and fault transmissivity. The power-law gives the best fit for three of the four conditions modelled, although exponential, logarithmic and cubic laws also fit the data well. As the power-law gave the best fit for the current data, especially in the early stages of loading, we propose this as a description of fault transmissivity with

289 stress. The colation of more datasets will give a better understanding of the relationship
290 between stress and fault flow.

291 Figure 4 shows the change in transmissivity with decreasing vertical stress during the first
292 unloading stage. As can be seen both kaolinite (Figure 4a) and Ball Clay (Figure 4c) show
293 similar behaviour with transmissivity essentially unchanged, even when vertical stress was
294 reduced to 0.07 MPa during test ASR_BigCCS_01. This demonstrates that the clay has
295 considerable hysteresis and "memory" of the maximum stress that was experienced. Figure
296 4c compares the results achieved for kaolinite and Ball Clay. Both clays give a good power-
297 law relationship with an exponent of -0.5, with variation in the base number; 4.44 and 2.59
298 for kaolinite and Ball Clay respectively. No significant variation in gouge thickness was
299 noted between the tests (see Figure 7c). Therefore the difference in the base number is related
300 to the difference in mineralogy between the two tests.

301 Figure 5 shows the complete data for test ASR_BigCCS_01 conducted on kaolinite gouge.
302 As can be seen, increasing vertical stress resulted in a reduction in flow. During reloading,
303 continued increases of vertical stress up to 6.45 MPa, the previous maximum vertical stress,
304 did not result in any further reduction in flow. As vertical stress increased to a new maximum
305 in the test history, transmissivity continued to decrease following a power-law relationship.
306 Vertical stress was increased to a maximum of 10 MPa, resulting in a transmissivity of $0.75 \times$
307 10^{-14} m^2 s^{-1}. As shown in Figure 4b, reloading of the fault does not result in any change in
308 transmissivity until a new maximum stress has been achieved. Close examination of all data
309 shows that the first stage of reloading, increasing vertical stress from 0.7 to 2 MPa resulted in
310 slip along the fault plane. This was detected as a slight change in shear stress and vertical
311 displacement. No other change in vertical stress resulted in a slip event. It is possible to
312 correct this influence, as shown by the black arrows in Figure 5b, with corrected reload data
313 shown by open diamond symbols. The resulting relationship is shown in Figure 5c, with a

power-law describing the reduction of flow properties during increasing vertical stress conditions and a linear constant relationship describing the behaviour when vertical stress was reduced.

Figure 6 shows the complete data for test ASR_BigCCS_02 conducted on Ball Clay gouge. As seen in Figure 6a and in more detail in Figure 6b, reloading followed a path similar to that seen during unloading. Transmivity data for unloading from 6.45 MPa to 0.42 MPa gives an average of 0.93×10^{-14} m^2 s^{-1} compared with an average of 0.91×10^{-14} m^2 s^{-1} during reloading from 0.42 MPa to 6.45 MPa. Therefore it can be concluded that flow is 'identical' during unloading and reloading and no change, either increase or decrease occurs. Throughout the unload-reload history the gouge has a memory of the maximum stress it has experienced. Only one further step was conducted after the previous maximum 6.45 MPa, therefore it cannot be determined if transmissivity continued to decrease as described by a power-law. However, as seen in Figure 6, the loading stages of the experiment are well described by a single power-law relationship. The second unload stage of the experiment resulted in no change in transmissivity.

Figure 7 shows the results of flow achieved for the two tests conducted injecting water into a 30° discontinuity during load-unload-reload-unload stages. As can be seen, the reduction in transmissivity (T) during increasing vertical stress (σ_v) can be described by power-law relationships. In all four stages with decreasing vertical stress it was seen that transmissivity remained constant and reloading resulted in no variation in flow unless slip or a new maximum stress state was achieved. Figure 7c shows the results for fracture thickness during the experiment. For kaolinite a general linear reduction in fracture width was seen, whereas in Ball Clay a form similar to that seen in flow was observed. This suggests that a component of

337 flow is related to fracture thickness, with an additional component related to the compaction
338 behavior of the clay gouge.

339 **4.0 Discussion**

340 The sequestration of super-critical carbon dioxide will result in pore pressure perturbations of
341 the injected reservoir. This will result in elevated pore pressure at faults, reducing effective
342 stress, and may result in super-critical CO_2 coming into contact with existing faults. The
343 current study utilized water as the injection fluid, so as to directly simulate the pressure pulse
344 of the reservoir within the existing pore fluid. The configuration of the angled shear rig did
345 not allow super-critical CO_2 to be injected; the injection of super-critical CO_2 at vertical
346 stress up to 10 MPa at 20° C would result in the instantaneous conversion to a gaseous form,
347 which would not occur in reality. However, the fluid nature of super-critical CO_2 should
348 behave similarly to water, although it may have an increased influence on flow as it reacts
349 with the clay gouge.

350 The current experimental study utilized a kaolinite or Ball Clay gouge as an analogue for a
351 clay-filled fault. This was in order to reduce the number of variables in the experiments by
352 effectively eliminating fracture roughness and the presence of asperities. The selection of
353 kaolinite was guided by the low swelling capacity of the clay, facilitating quicker
354 experiments and the study of a greater number of features of fracture flow. Ball Clay was
355 selected as it has a kaolinite content of 37 %, along with 35 % illite and 26 % quartz. This
356 was deemed to be sufficiently different in terms of mineralogy than pure kaolinite to observe
357 whether mineralogy played a role on fracture flow properties and behavior. If such an
358 observation was made then further research would be needed to fully quantify the role of
359 mineralogy on fault flow behavior.

Comparisons can be seen between the current experiments and those conducted on fractures in Opalinus Clay (OPA). Cuss *et al.* [2009; 2011] describe the variation of fracture flow dependence on normal stress for an idealized planed fracture. A hydraulic transmissivity of approximately 5×10^{-14} $m^2.s^{-1}$ was observed in OPA, which is comparable with the $0.5 – 5 \times 10^{-14}$ $m^2.s^{-1}$ seen in the current study. Fracture transmissivity in a realistic fracture in OPA has been shown to reduce in a similar form to the current study [Cuss *et al.*, 2012; 2014[1,2]]. These observations therefore show that the use of a kaolinite or Ball Clay gouge can be seen to have been justified given the similarity seen in response.

It was seen in test ASR_BigCCS_01 that flow reduced during the first step of reloading, possibly as a result of shear. Fracture transmissivity was seen to reduce in OPA as a result of shear for a planed fracture [Cuss *et al.*, 2009; 2011] and for a realistic fracture [Cuss *et al.*, 2012; 2014[1,2]]. Cuss *et al.* [2014[1]; 2014[2]] showed that shear reduced fracture transmissivity by approximately one order of magnitude. Cuss *et al.* (2013) also showed that shear was an effective self-sealing mechanism in kaolinite paste with a 40 % reduction in flow seen as a result of shear. This compares with the 60 % reduction in flow seen during test ASR_BigCCS_01. The fracture width and vertical displacement data suggest that movement did occur, although movement was of the order of 10's microns. Previous studies have shown that active shearing is an effective self-sealing mechanism that occurs in naturally fractured claystone, such as Opalinus Clay, and in clay gouge material, such as kaolinite. The current data suggest that only small shear movements are sufficient to alter the flow properties of clay-rich gouge. This is not too surprising given the nano- to micro-scale of clay minerals. As no further movements along the fracture plane were observed, the correction of the transmissivity data shown in Figure 5b was possible to remove the influence of shear. Therefore it is suggested that a small slip event occurred as vertical stress was increased by 2 MPa, which resulted in a reduction of flow properties.

385 The current study has highlighted the significance of stress history. The behavior observed
386 during unloading was similar for both tests during all four unloading stages. Considerable
387 hysteresis was seen during the unloading cycles of the test history with transmissivity
388 remaining constant with a memory of the maximum load experienced. Similar hysteresis has
389 been noted in Opalinus Clay [Cuss *et al.* 2009; 2011]; whilst the data were not described in
390 terms of hysteresis, a reinterpretation of the data shows that hysteresis was indeed observed.
391 This illustrates the importance of stress history on predicting flow along discontinuities and
392 has been used to explain the non-applicability of the critical stress approach in its simple
393 form at the Sellafield site in the UK [Sathar *et al.*, 2012]. Therefore stress history is an
394 important control on fracture flow and consideration only of the current stress state will lead
395 to inaccuracies of the flow of fractured rocks.

396 During unloading and reloading it can be argued that the amount of flow recovered is
397 effectively zero, even when vertical stress is reduced to very small magnitudes. During
398 unloading of a deformed sediment only the elastic deformation is recovered and the stress
399 path followed corresponds to the rebound-reconsolidation line (RRL) or the swelling-
400 recompression line (SRL) under drained conditions. The form of the flow seen during cyclic
401 loading suggests that the clay paste follows the normal consolidation line (NCL) during
402 loading, with considerable hysteresis seen as the clay follows the SRL during unloading and
403 reloading, until the NCL is once again reached, from where the plastic deformation occurs,
404 following the NCL. The NCL and RRL are usually defined in the effective stress versus void
405 ratio (e) space, therefore fracture transmissivity observed is related to the change in void ratio
406 as the gouge consolidates in response to the vertical stress. This consolidation takes the form
407 of a power-law relationship. However, as shown in Table 3, an exponential, cubic or
408 logarithmic fit can also achieve satisfacory fits to the data. The power-law relationship gives
409 the best fit to the data in the early stages of initial loading, as shown in Figure 8..

The load-unload-reload-unload experiments conducted on kaolinite and Ball Clay did not significantly vary. The form of the transmissivity reduction with vertical stress was similar, with differences noted in the fracture transmissivity seen at 6.5 MPa. This difference may simply be related to differences in permeability of the two gouges and differences in gouge thickness, although as shown in Figure 7c, the two tests achieved similar gouge thickness. The illite content of Ball Clay is likely to have a lower permeability, as observed as a lower fracture transmissivity. It should also be noted that the Ball Clay gouge resulted in a more pronounced reduction in transmissivity with increased vertical stress; this will be related to the differences in grain dimension, swelling potential, and permeability of the two gouge materials. The minimum transmissivity seen after both clay gouges had been loaded to 10 MPa vertical stress was approximately 0.8 and 1.5×10^{-14} m^2 s^{-1} for Ball Clay and kaolinite respectively. Therefore the variation in mineralogy had resulted in variations in the power-law reduction in flow and transmissivity at increased vertical stress, but did not alter the unloading behaviour.

Faults within clay-rich caprock seals are likely to be of low permeability and this will affect the drainage of the gouge during loading and unloading cycles. The current experiments were all conducted as drained experiments, with a central 1 MPa pore pressure reducing to atmospheric pressure at the outside of the sample. If the gouge was behaving as undrained, it would be expected to see pore pressure increases at P1 and P2 as vertical stress was increased. Modelling of the radial pressure distribution expected from such a geometry predicts that pore pressure should be 250 kPa at the observation pressure ports,as shown in Figure 9. This is greatly in excess of the measured pore pressure, which had a maximum of 35 kPa. This either suggests that pore pressure was not simply radial flow, or that channelised flow occurred. Cuss *et al.* (2011) used flurocene tagged water to show that fracture flow in Opalinus Clay exploited less than 50 % of the total fracture surface. This test was conducted

under static boundary conditions for over 100 days and attained full steady-state conditions; therefore the localisation of flow and low pore pressure within the gouge cannot be simply due to non-steady state flow. It is therefore possible that hydraulic flow is simply not intersecting the two pore pressure monitoring locations. The use of an inclined fault plane at 30° would likely result in preferential flow down-dip, however, the location of P2 suggests that this is not the case. This suggests that the dip of the plane plays little role on the flow direction of the injected fluid. Unfortunately it is not possible to retrieve the gouge at the end of the experiment to determine where fluid flow has been active. In nature the conditions are likely to be drained, but if the stress change is rapid compared with the drainage rate, the response may be akin to undrained testing. The observations seen of hysteresis during unloading and the description of the stress path followed as an RRL response is likely to occur under undrained conditions. However, increses in vertical stress are likely to create elevated pore pressures, which results in a more complex permeability response with changes in vertical stress.

5.0 Conclusions

This paper describes an experimental study of 2 load-unload-reload experiments, both on a 30° slip-plane filled with kaolinite or Ball Clay gouge. The main conclusions of the study were;

a. The transmissivity of the Ball Clay and kaolinite gouge showed a power-law relationship with stress between 0 and 10 MPa vertical stress.
b. During a loading (vertical stress) and unloading cycle considerable hysteresis in flow was observed signifying the importance of stress history on fracture flow. Consideration of just the current stress acting upon a fracture may result in inaccuracies of predicted water flow;

c. During reloading a permeability response akin to the rebound-reconsolidation line was observed until a stress state equivalent to the maximum stress experienced previously, from where flow continued to reduce as the response now followed the normal consolidation line.

d. Shear movement is an effective self-sealing mechanism that can reduce the transmissivity of fractures with only small movements of the order of 10's microns needed to reduce transmissivity.

e. No significant variation was seen in the relationship between stress and flow between kaolinite and Ball Clay, with both well described by a power-law. This suggests the inclusion of illite and quartz did not have a significant alteration to the relationship between stress and flow. Ball Clay is likely to have a lower permeability than pure kaolinite and this was observed as a lower fracture transmissivity, as seen by the power-law coefficients.

f. Observations of flow within a clay-filled gouge were consistent with experiments conducted on Opalinus Clay, showing that the simplified experimental geometry effectively replicated the flow observed in real fractures.

Acknowledgements

The study was undertaken by staff of the Minerals and Waste Program of the BGS using the experimental facilities of the Transport Properties Research Laboratory (TPRL). The authors would like to thank the skilled staff of the Research & Development Workshops at the BGS, in particular Humphrey Wallis, for their design and construction of the experimental apparatus. This publication has been produced with support from the BIGCCS Centre. The BIGCCS Centre is part of the Norwegian research programme Centres for Environment-friendly Energy Research (FME) and is funded by the following partners: Aker Solutions, ConocoPhillips, Det Norske Veritas, Gassco, Hydro, Shell, Statoil, TOTAL, GDF SUEZ and

the Research Council of Norway (193816/S60). The BGS authors publish with the permission of the Executive Director, British Geological Survey (NERC).

References

Cuss, R.J., Sathar, S., and Harrington, J.F. (2013) Final Report of FORGE WP4.1.2: Validation of critical stress theory applied to repository concepts. *British Geological Survey Commissioned Report*, **CR/13/001**. 96pp.

Cuss, R.J., Milodowski, A.E., Harrington, J.F. and Noy, D.J. (2009) Fracture transmissivity test of an idealised fracture in Opalinus Clay. British Geological Survey Commissioned Report, CR/09/163. 74pp.

Cuss, R.J., Milodowski, A., and Harrington, J.F. (2011) Fracture transmissivity as a function of normal and shear stress: first results in Opalinus clay. Physics and Chemistry of the Earth. 36, pp. 1960-1971.

Cuss, R.J., Harrington, J.F., Milodowski, A.E., and Wiseall, A.C. (2014[a]). Experimental study of gas flow along an induced fracture in Opalinus Clay. British Geological Survey Commissioned Report, CR/14/051. 79pp.

Cuss, R.J. and Harrington, J.F. (2014[b]) Experimental observations of the flow of water and gas along fractures in Opalinus Clay. Extended abstract We07. Fourth EAGE Shale Workshop, 6-9 April 2014, Porto, Portugal.

Cuss, R.J., Harrington, J.F., Sathar, S., and Norris, S. (2015) An experimental study of the flow of gas along faults of varying orientation to the stress-field; Implications for performance assessment of radioactive waste disposal. Journal of Geophysical Research – Solid Earth. 120, pp.3932-3945, doi:10.1002/2014JB011333

David, C., Wong, T.F., Zhu, W., and Zhang, J. (1994) Laboratory measurement of compaction-induced permeability change in porous rocks; implications for the generation

508 and maintenance of pore pressure excess in the crust. Pure and Applied Geophysics, 143,
509 pp. 425-456.

510 Dewhurst, D.N., Aplin, A.C., and Sarda, J.-P. (1999) Influence of clay fraction on pore-scale
511 properties and hydraulic conductivity of experimentally compacted mudstones. Journal of
512 Geophysical Research, 104, pp. 29,261-29,274.

513 Dewhurst, D.N., Aplin, A.C., Sarda, J.-P., and Yang, Y. (1998) Compaction-driven evolution
514 of porosity and permeability in natural mudstones: An experimental study. Journal of
515 Geophysical Research, 103, pp. 651-661.

516 Dewhurst, D.N., Yang, Y., and Aplin, A.C. (1999) Permeability and fluid flow in natural
517 mudstones. In: Aplin, A.C., Fleet, A.J., and Macquaker, J.H.S., eds., Mud and Mudstones:
518 Physical and Fluid Flow Properties, Geological Society of London, Special Publications,
519 158, pp. 23-43.

520 Donohew, A.T., Horseman, S.T., and Harrington, J.F. (2000) Gas entry into unconfined clay
521 pastes at water contents between the liquid and plastic limits. in: Environmental
522 Mineralogy: Microbial Interactions, Anthropogenic Influences, Contaminated Land and
523 Waste Management; Cotter-Howells, J.D., Campbell, L.S., Valsami-Jones, E., and
524 Batchelder, M. (eds). *Mineralogical Society Series*, **9**. Mineralogical Society, London. Pp.
525 369-394 ISBN 0 903056 20 8.

526 Espinoza, D. Nicolas, and J. Carlos Santamarina. (2012). Clay interaction with liquid and
527 supercritical CO2: The relevance of electrical and capillary forces." International Journal of
528 Greenhouse Gas Control, 1, 351-362.

529 Green, C., Styles, P. and Baptie, B. (2011). Preese Hall Shale gas fracturing review and
530 recommendations for induced seismic mitigation, Independent Review, Pub. Department of
531 Energy and Climate Change, UK.

532 Gutierrez, M., Øino, L.E. and Nygard, R. (2000) Stress-dependent permeability of a de-
533 mineralised fracture in shale. Marine and Petroleum Geology, 17, pp.895–907.
534 Highley, D.E. (1984) China Clay. Mineral Dossier No. 26. Mineral Resources Consultative
535 Committee, HMSO, London.
536 Holt RM (1990) Permeability reduction induced by a non-hydrostatic stress field. SPE
537 Formation Evaluation, Dec 1990, pp. 444–448
538 Horseman, S. T., R. J. Cuss, and H. J. Reeves. (2005). Clay Club initiative: Self-healing of
539 fractures in clay-rich host rocks. In 'Stability and Buffering Capacity of the Geosphere for
540 Long-term Isolation of Radioactive Waste', Nuclear Energy Agency 117.
541 Katsube, T.J., Issler, D.R., and Coyner, K. (1996) Petrophysical characteristics of shale from
542 the Beaufort-Mackenzie Basin, northern Canada; permeability, formation factor, and
543 porosity versus pressure, Interior plains and Arctic Canada. Current Research - Geological
544 Survey of Canada. pp. 45-50.
545 Katsube, T.J., Boitnott, G.N., Lindsay, P.J., and Williamson, M. (1996) Pore structure
546 evolution of compacting muds from the seafloor, offshore Nova Scotia. In: Anonymous,
547 ed., Eastern Canada and national and general programs. Current Research - Geological
548 Survey of Canada, pp. 17-26.
549 Katsube, T.J. (2000) Shale permeability and pore-structure evolution characteristics.
550 Geological Survey of Canada. Ottawa, ON, Canada. Pages: 9.
551 Keaney, G.M.J., Meredith, P.G., and Murrell, S.A.F. (1998) Laboratory study of permeability
552 evolution in a 'tight' sandstone under non-hydrostatic stress conditions. Rock Mechanics in
553 Petroleum Engineering, 1 8-10 July 1998, Trondheim, Norway, Society of Petroleum
554 Engineers, SPE/ISRM 47265, pp. 329-335.

555 Kwon, O., Kronenberg, A.K., Gangi, A.F., and Johnson, B. (2001) Permeability of Wilcox
556 Shale and its effective pressure law. Journal of Geophysical Research, B, Solid Earth and
557 Planets, 106, pp. 19,339-19,353.

558 Morrow, C., Shi, L.Q., and Byerlee, J.D. (1984) Permeability of fault gouge under confining
559 pressure and shear stress. Journal of Geophysics Research, 89, pp. 3193-3200.

560 Neuzil, C.E., Bredehoeft, J.D. and Wolff, R.G. (1984) Leakage and fracture permeability in
561 the Cretaceous shales confining the Dakota aquifer in South Dakota. In: Proceedings of
562 First C.V. Theis Conference on Geohydrology in Dublin, Ohio. Jorgensen, D.G. and Signor,
563 D.C. (eds.). National Water Well Association. pp.113-120.

564 Noy, D.J.,Holloway, S., Chadwick, R.A., Williams, J.D.O., Hannis, S.A. and Lahann, R.W.
565 (2012). Modelling large-scale carbon dioxide injection into the Bunter Sandstone in the UK
566 Southern North Sea. International Journal of Greenhouse Gas Control, 9, 220–233.

567 Sathar, S., Reeves, H.J., Cuss, R.J., and Harrington, H.J. (2012) Critical stress theory applied
568 to repository concepts; the importance of stress tensor and stress history in fracture flow.
569 Mineralogical Magazine. December 2012, 76 (8), pp. 3165-3177.

570 Schloemer, S., and Krooss, B.M. (1997) Experimental characterisation of the hydrocarbon
571 sealing efficiency of cap rocks. Marine and Petroleum Geology, 14, pp. 565-580.

572 Tsang, C.-F., Bernier, F. and Davies, C. (2005). Geohydromechanical processes in the
573 Excavation Damaged Zone in crystalline rock, rock salt, and indurated and plastic clays—in
574 the context of radioactive waste disposal, International Journal of Rock Mechanics &
575 Mining Sciences 42, 109–12.

576 Walsh, J.B., and Brace, W.F. (1984) The effect of pressure on porosity and the transport
577 properties of rock. Journal of Geophysical Research. B, 89, pp. 9425-9431.

578 Zhu, W., and Wong, T.f. (1994) Permeability evolution related to the brittle-ductile transition
579 in Berea Sandstone. In: Anonymous, ed., AGU 1994 fall meeting., 75; 44 Suppl.: Eos,
580 Transactions, American Geophysical Union. pp. 638.

581 Zhu, W., and Wong, T.-f. (1997) The transition from brittle faulting to cataclastic flow;
582 permeability evolution. Journal of Geophysical Research, B, Solid Earth and Planets, 102,
583 pp. 3027-3041.

584 Zoback, M.D., and Byerlee, J.D. (1975) The effect of microcrack dilatancy on the
585 permeability of Westerly Granite. Journal of Geophysics Research, 80, pp. 752-755.

586 Zoback, D. and Gorelick, S. (2012). Earthquake triggering and large-scale geologic storage
587 of carbon dioxide. Proceedings of the National Academy of Sciences 109.26 (2012): 10164-
588 10168.

589

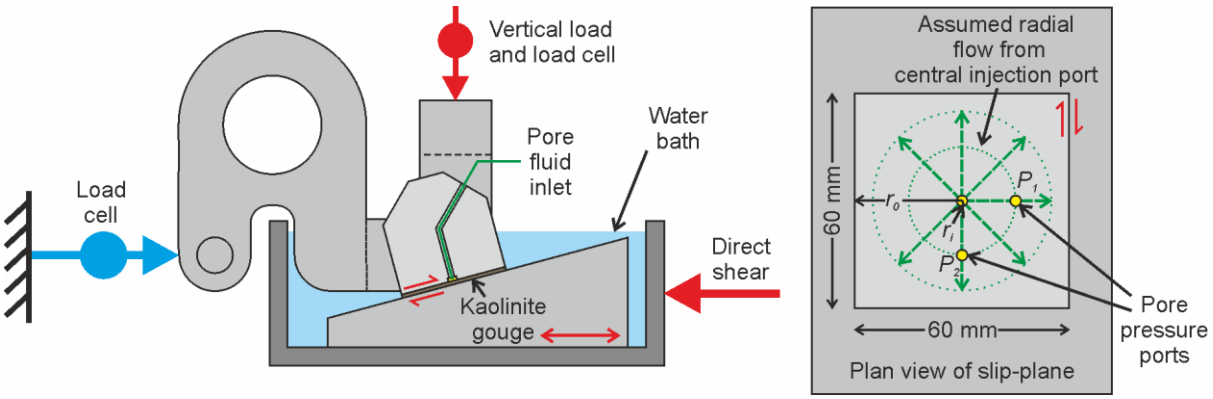

590 **Figure 1** Schematic of the Angled Shear Rig (ASR).

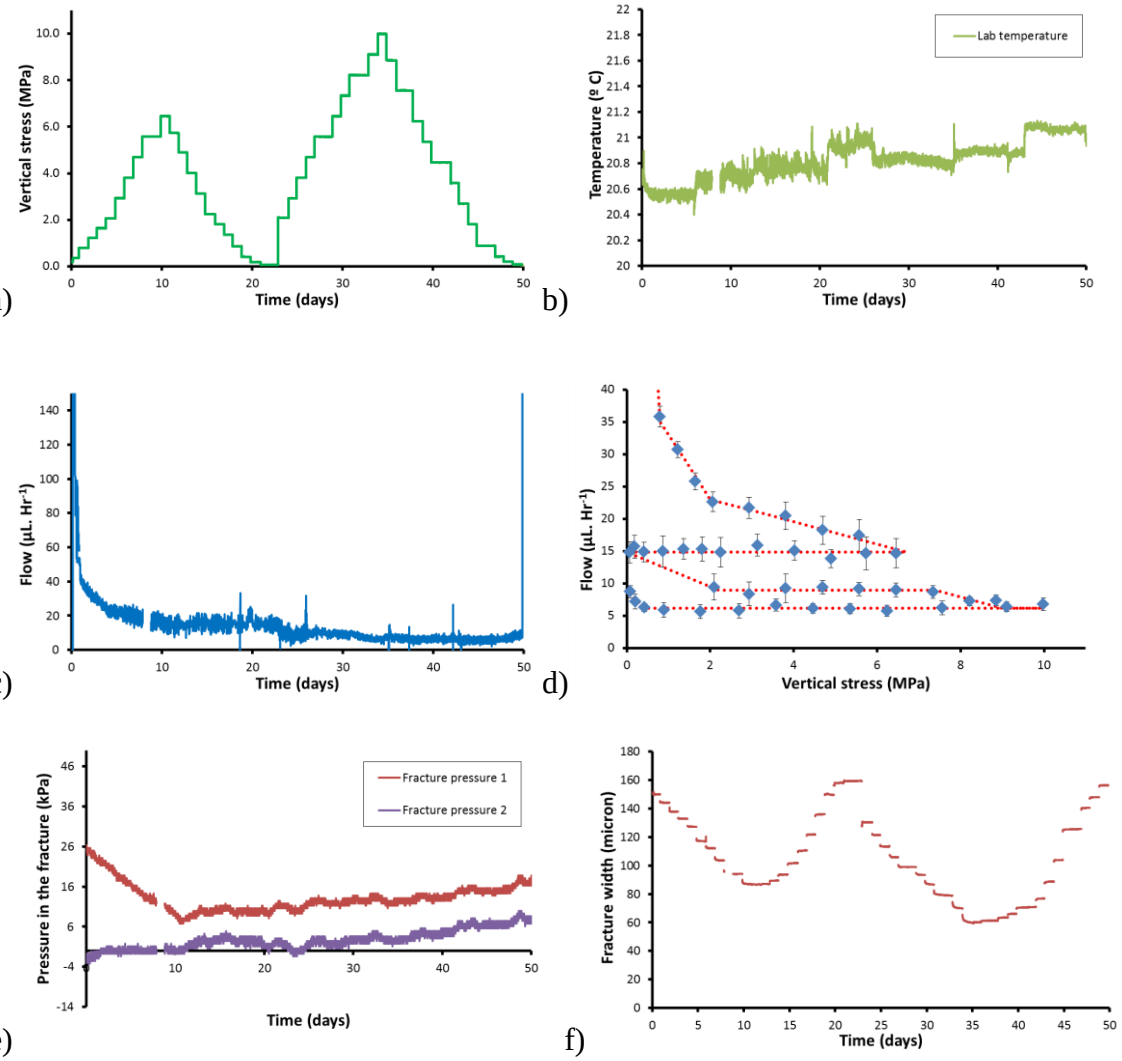

Figure 2 Results from load-unload-reload-unload (LURU) test conducted on kaolinite (ASR_BigCCS_01): a) vertical stress; b) temperature; c) hydraulic flow with time; d) hydraulic flow variation with vertical stress; e) pore pressures within the slip plane at pore pressure ports P_1 and P_2; f) Fracture width.

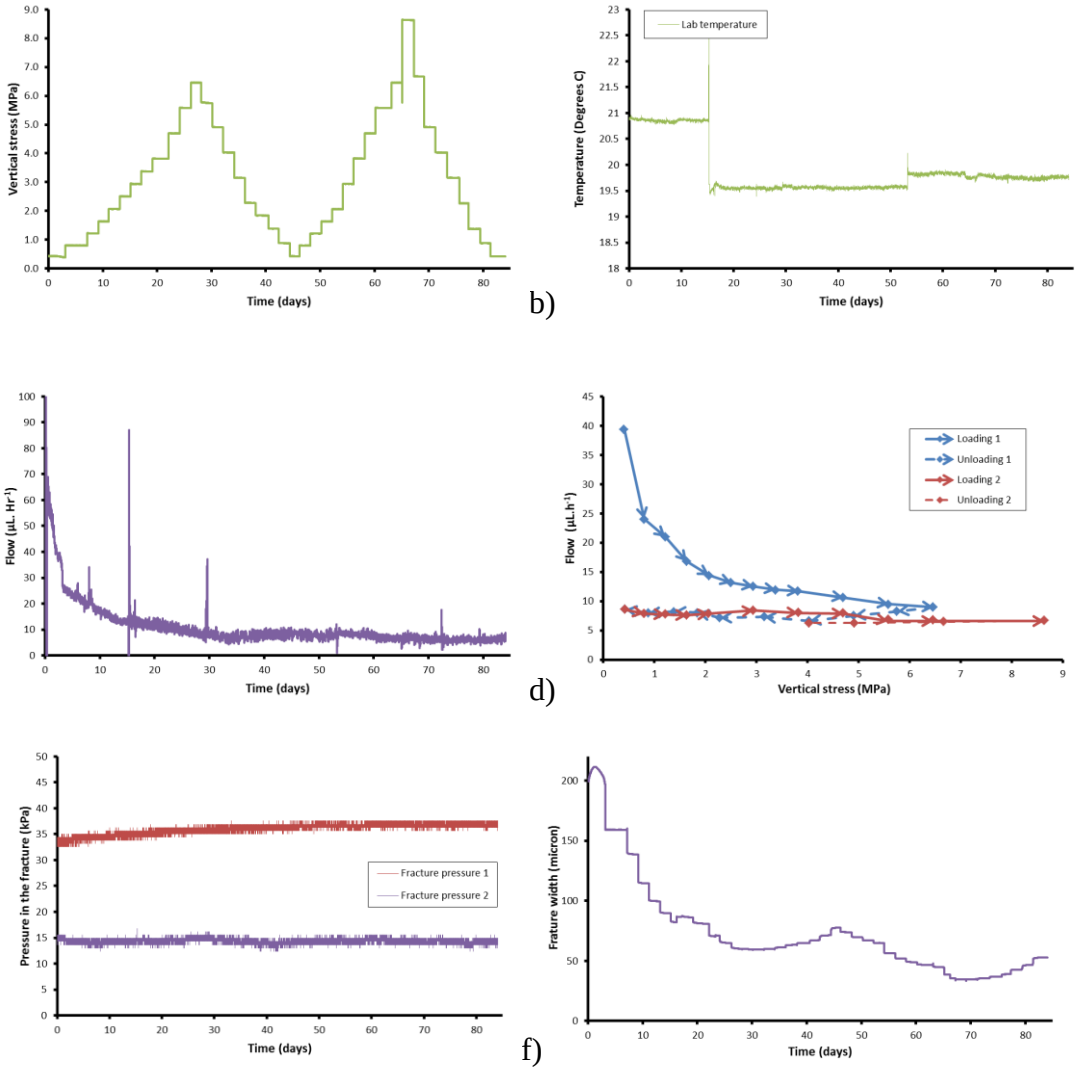

Figure 3 Results from load-unload-reload-unload (LURU) test conducted on Ball Clay (ASR_BigCCS_02): a) vertical stress; b) temperature; c) hydraulic flow with time; d) hydraulic flow variation with vertical stress; e) pore pressures within the slip plane at pore pressure ports P_1 and P_2; f) Fracture width.

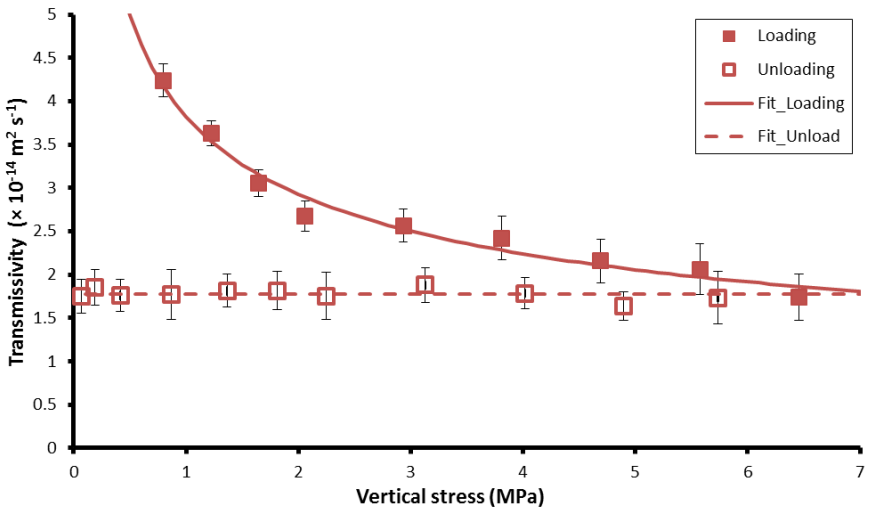

605 a)

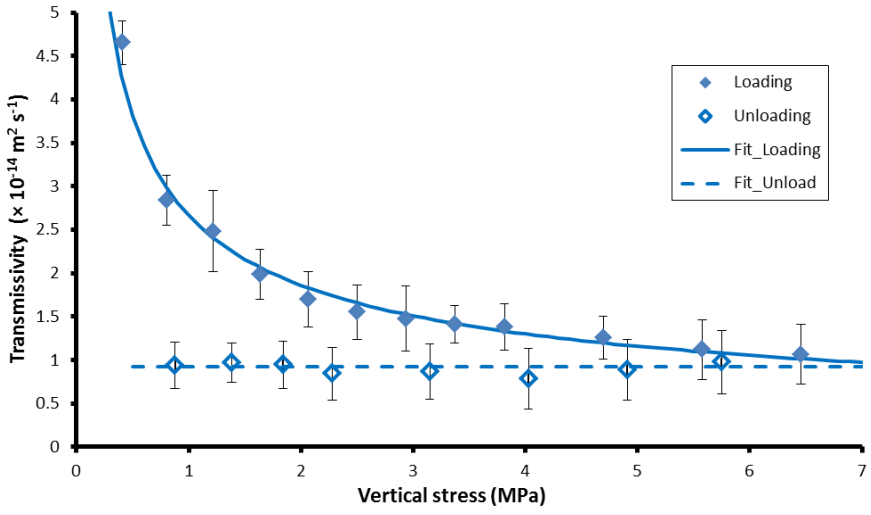

606 b)

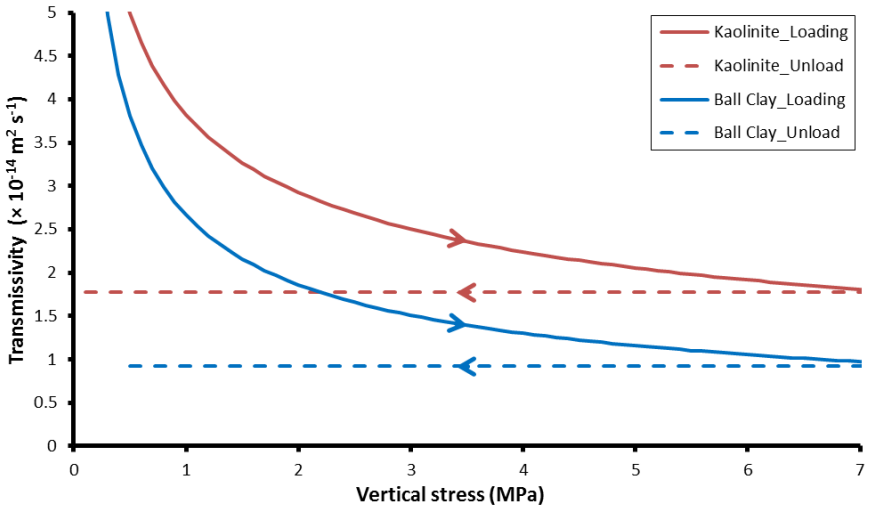

607 c)

608 **Figure 4** Example of hysteresis seen in flow during loading/unloading experiments on a
609 30° slip-plane; a) kaolinite loading-unloading experiments; b) Ball Clay during loading-
610 unloading-reloading experiments; c) comparison of kaolinite and Ball Clay during LU stages.

611 Note that error bars show the standard deviation observed in flow recorded over a 6 hour
612 period. This plot shows that flow reduces with increased load, but does not recover flow
613 during unloading.

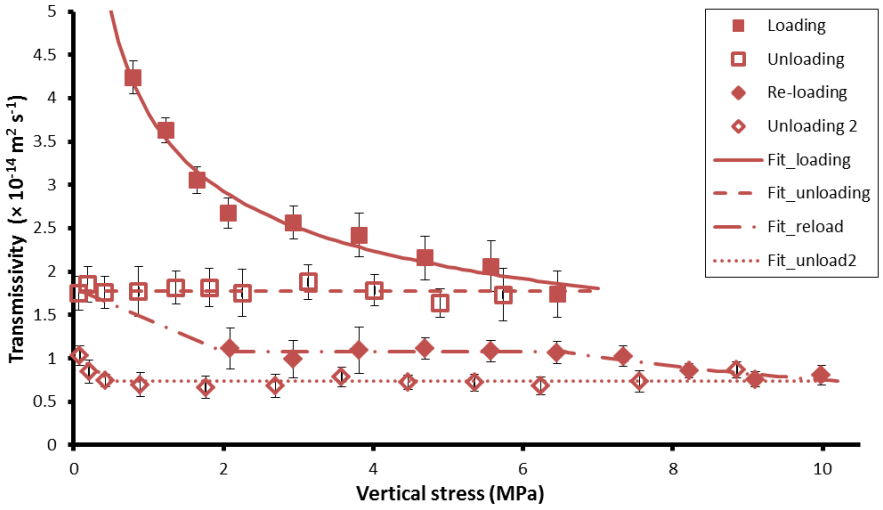

614 a)

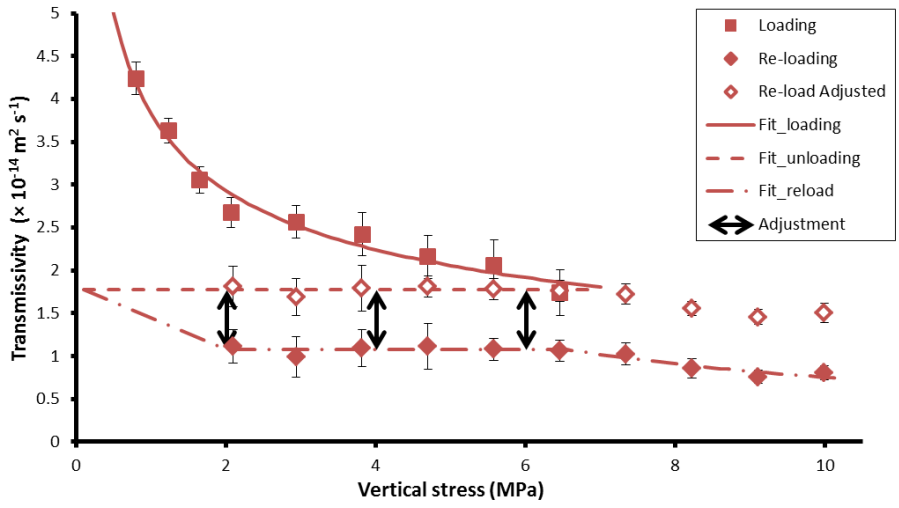

615 b)

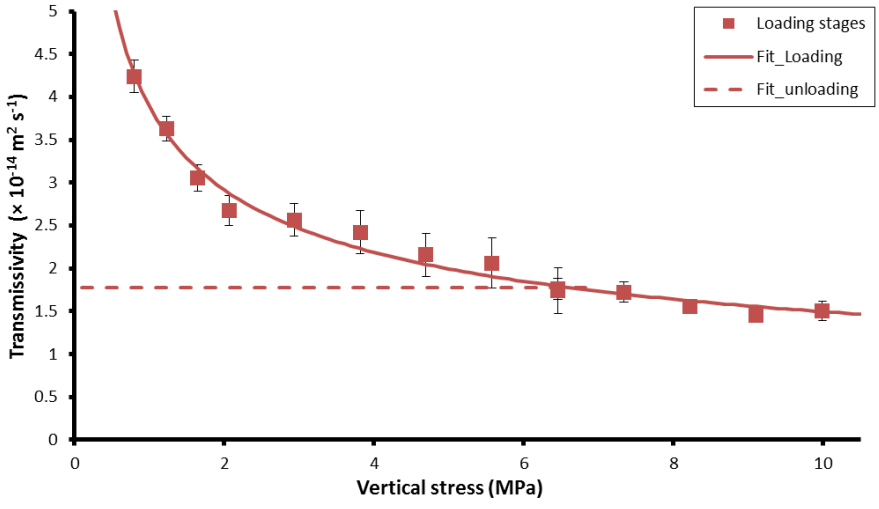

616 c)

617 **Figure 5** Results for reloading-unloading for test ASR_BigCCS_01 conducted on kaolinite
618 gouge; a) complete transmissivity data; b) adjustment of reloading data (see text for
619 explanation); c) adjusted results for complete LURU test. Note that error bars show the

620 standard deviation observed in flow recorded over a 6 hour period. This plot shows no
621 increase in flow occurs during until a new maximum stress has been attained, demonstrating
622 that fault flow has a stress memory.

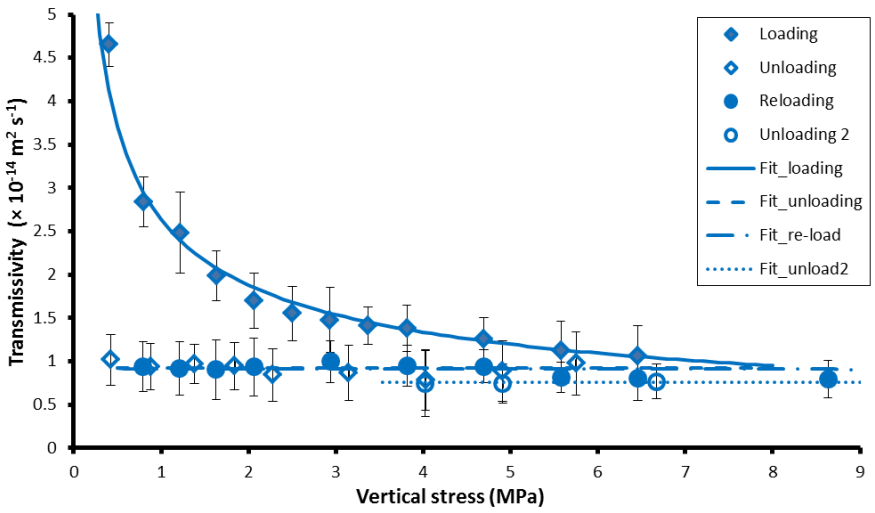

623 a)

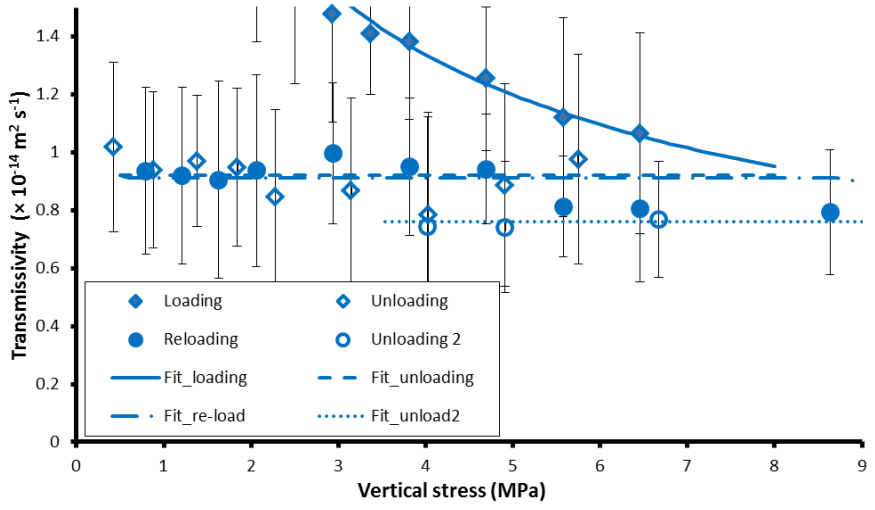

624 b)

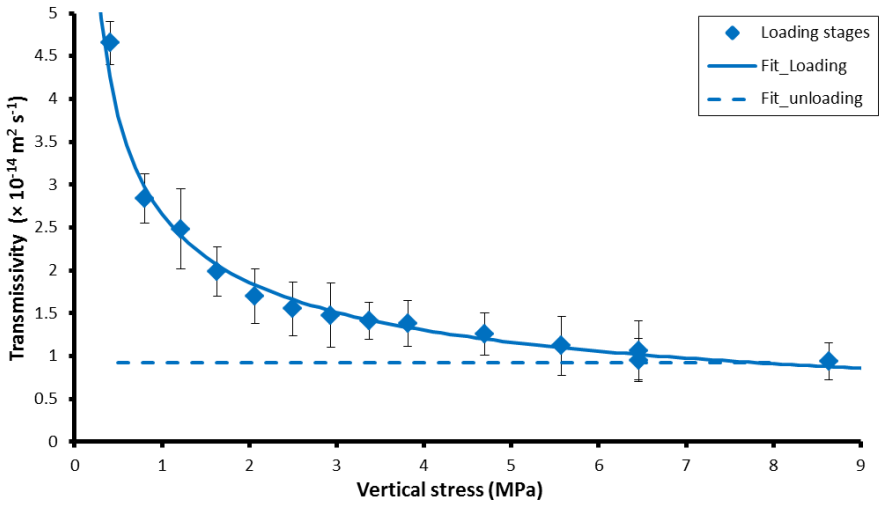

625 c)

626 **Figure 6** Results for reloading-unloading for test ASR_BigCCS_02 conducted on Ball
627 Clay gouge; a) complete transmissivity data; b) detail of unloading and reloading stages; c)
628 results for complete LURU test. Note that error bars show the standard deviation observed in

flow recorded over a 6 hour period. This plot shows no increase in flow occurs during until a new maximum stress has been attained, demonstrating that fault flow has a stress memory.

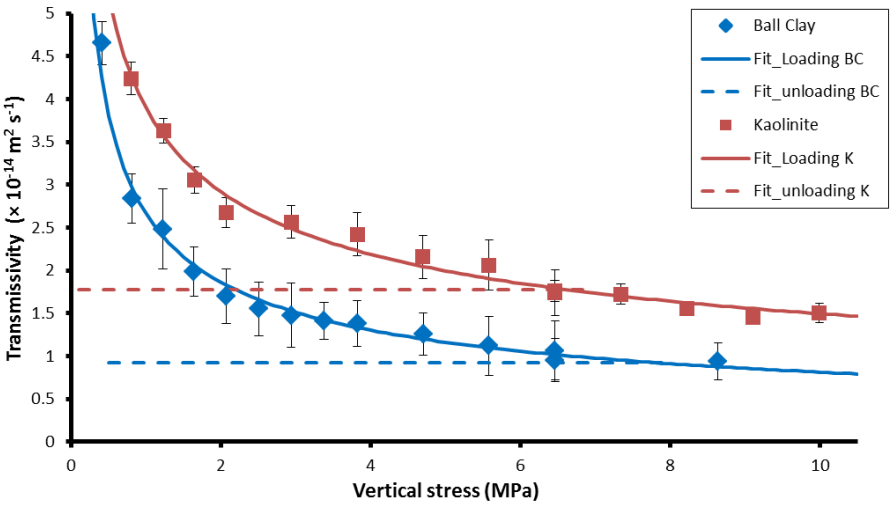

631 a)

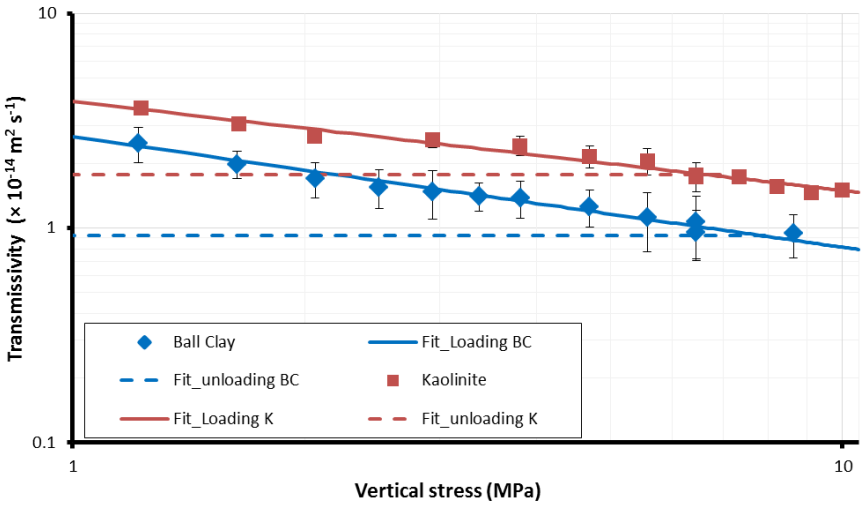

632 b)

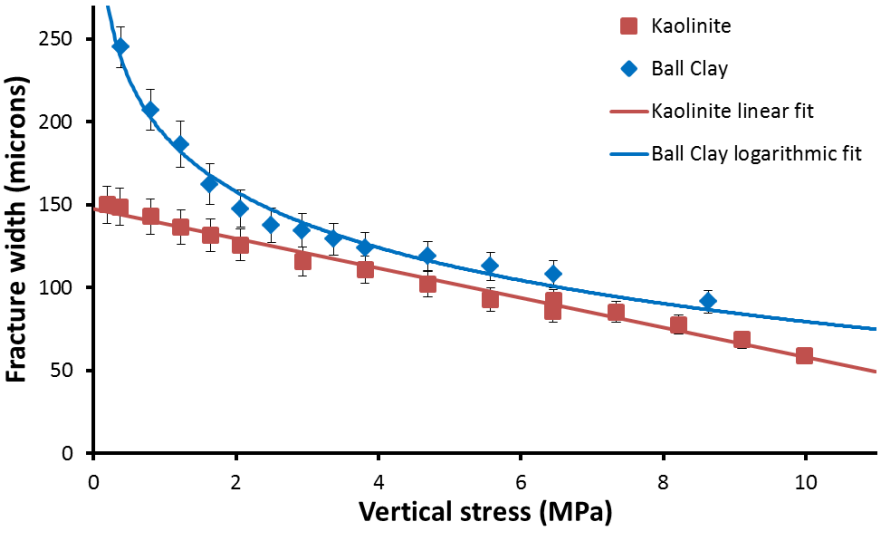

633 c)

Figure 7 Comparing the loading-unloading-reloading response of kaolinite and Ball Clay fault gouge material; a) power-law reduction in transmissivity seen during loading and stable flow seen during unloading; b) data shown in the log-log space giving linear relationships of transmissivity versus vertical stress; c) fracture width recorded during the experiment. Note that error bars show the standard deviation observed in flow recorded over a 6 hour period. This plot shows that loading can be represented by a power-law relationship, whilst unloading shows no change in flow properties.

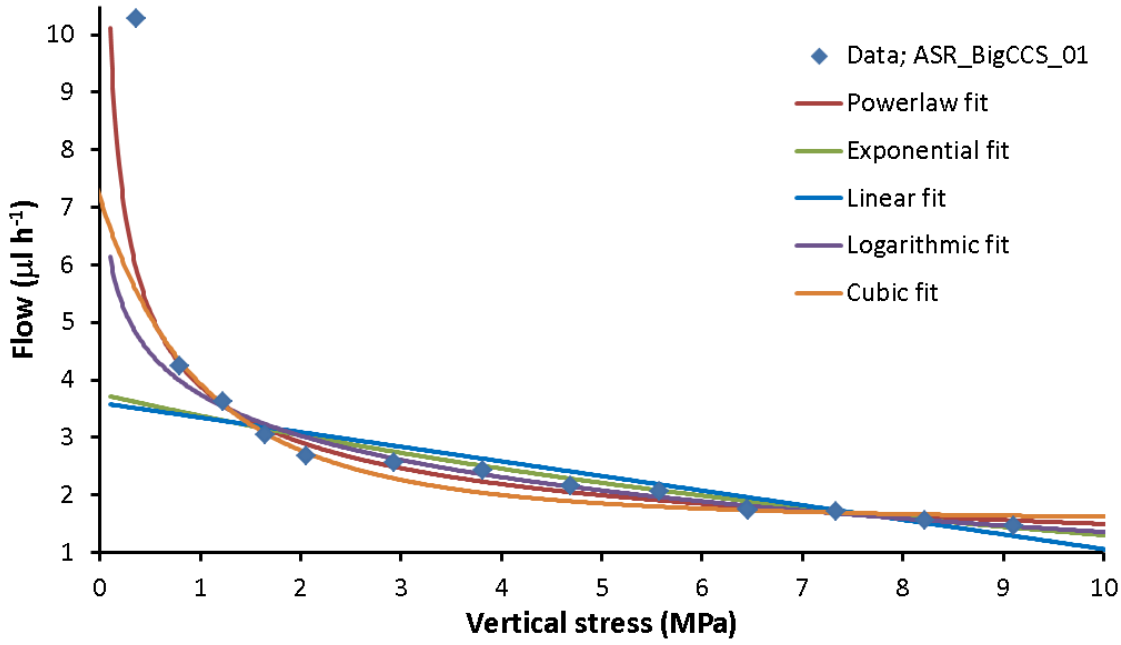

641

642 **Figure 8** Comparing five best-fit relationships to the experimental data of test
643 ASR_BigCCS_01. The power-law fit is seen to best describe the data, especially at the initial
644 loading stage at low vertical stress.

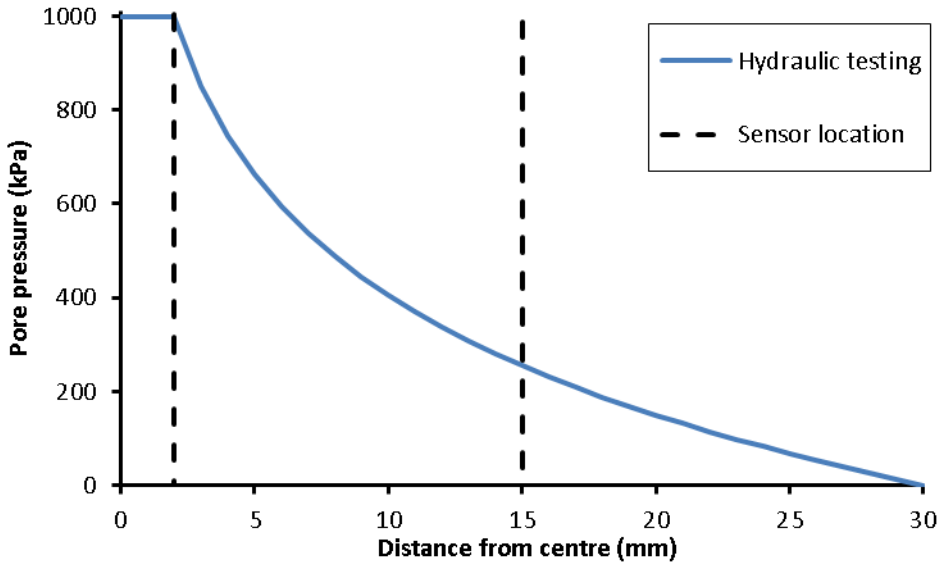

645

646 **Figure 9** Model of pore-pressure distribution in the clay gouge assuming radial flow.

Gouge	Supplier	Geological information	Location	Composition
Kaolinite	Imerys	well-ordered form, coarse hexagonal platelets[1]	St Austell, UK	100 % kaolinite
Ball Clay	Imerys	A1 seam; Tertiary, Poole Formation, Oakdale Clay Member)	Arne Clay Pit, Wareham, UK	37% kaolinite, 35% mica/illite and 26% quartz, together with some feldspar[2]

647 **Table 1** Description of the clay gouge materials used during the current study. [1] Highley,
648 (1984): [2] Donohew et al. (2000).

	Experiment	Sample Material	Type of test	Slip-plane orientation
1	ASR_BigCCS_01	Kaolinite	LURU	30°
2	ASR_BigCCS_02	Ball Clay		

649 **Table 2** List of all experiments undertaken as part of the current study. ASR = Angled

650 Shear Rig; LURU = load-unload-reload-unload experiment.

Test	Material	Section	Cubic	Exp	Linear	Log	Power
ASR_BigCCS_01	Kaolin	Load-reload	0.865	0.925	0.835	0.972	**0.979**
ASR_BigCCS_01	Kaolin	Unload	0.1	**0.2**	0.197	0.07	0.073
ASR_BigCCS_02	Ball Clay	Load-reload	0.973	0.783	0.573	0.888	**0.985**
ASR_BigCCS_02	Ball Clay	Unload	0.119	0.001	0.003	0.039	**0.045**

651 **Table 3**. Statistics for fit of data using different relationships. Values in bold represent the
652 best fit achieved.